IEEE Access
Multidisciplinary | Rapid Review | Open Access Journal

Received July 8, 2020, accepted July 21, 2020, date of publication July 28, 2020, date of current version August 12, 2020.

Digital Object Identifier 10.1109/ACCESS.2020.3012527

Generalized L-Shaped Array Based on the Difference and Sum Coarray Concept

XIANGNAN LI, XIAOHUA WANG, WEIJIANG WANG, AND SHIWEI REN
School of Information and Electronics, Beijing Institute of Technology, Beijing 100081, China

Corresponding author: Shiwei Ren (renshiwei@bit.edu.cn)

This work was supported by the National Natural Science Foundation of China under Grant 61801024.

ABSTRACT L-shaped array (LA) is traditionally used as two one-dimensional uniform linear arrays (ULAs) for two-dimensional direction of arrival (DOA) estimations. With elevation and azimuth angles estimated separately, the detectable source number is strictly limited by the number of elements in the ULAs. To increase the detection ability, in this paper, we propose to exploit the diff-sum co-array (DSCA) concept on the L-shaped array. As such, a virtual element in the quadrants of DSCA can be generated by only one pair of sensors in the LA. Therefore, it can acquire much higher number of degrees of freedom for DOA estimation. To further reduce the redundancy of elements on the horizontal and vertical axes of DSCA, an element moving strategy is proposed. It is proved that the DSCA can remain intact with any one or more physical sensors relocated to the centrosymmetric positions. Based on this strategy, a generalized L-shape array concept and a new configuration referred to as generalized L-shaped array with odd-even locations (GLA-OEL) are developed. For GLA-OEL, the number of sensor pairs with small spacing is as small as one, which dramatically reduces the mutual coupling of adjacent elements. Besides, with the same number of sensors, the GLA-OEL can generate much larger virtual uniform rectangular array in the DSCA. Simulations verify the superiorities of the proposed array in terms of detection performance and estimation accuracy.

INDEX TERMS Generalized L-shaped array, DOA estimation, Diff-sum co-array, degree of freedom, mutual coupling.

I. INTRODUCTION

Direction of arrival (DOA) estimation plays a critical role in many applications such as radar, wireless communications and radio astronomy [1], [2]. Conventional DOA estimation techniques are mainly based on uniformly and regularly placed physical geometries including uniform linear arrays (ULA), uniform circular arrays and uniform rectangular arrays (URA) [1]. Sensors in these structures are densely positioned, leading to considerable mutual coupling effect and significant reduction of resolution [3]–[5].

To enlarge the sensor spacings between adjacent elements, many one-dimensional (1D) sparse arrays have been developed. One of the well known non-uniform linear arrays (NLAs) is the minimum redundancy array (MRA) [6]. MRA is verified optimal in large consecutive difference segment achievement. However, it is obtained by going through every possibility of sensor locations by computer instead of having analytical expression. Moreover, the number of sensors can not exceed 17, which dramatically limits the use of MRA. The recent proposed nested array [7] and coprime array [8] attract more interest in NLA design. Such configurations have closed-form expressions of sensor locations. By vectorizing the covariance matrix of the received data and utilizing the spatial smoothing [9], the difference co-array (DCA) can be generated. Therefore, $O(N^2)$ degrees of freedom (DOF) can be achieved with only $O(N)$ sensors used. For further improvement of DOF, the augmented nested array (ANA) [10], improved nested array [11], array configuration based on the maximum inter-element spacing constraint (MISC) [12],the enhanced nested array [13], the extended nested array [14] and generalized coprime arrays [15] are proposed. With the mutual coupling effect considered, super nested arrays [16], [17] and ANA [10] are developed. Furthermore, combined with other different signal models, a series of virtual array based configurations are also developed [18]–[21]. According to the above 1D sparse array, several coarray-based DOA estimation algorithms are proposed recently. In [22], spatial smoothing PAST algorithm is proposed by exploiting the aperture of difference coarray

The associate editor coordinating the review of this manuscript and approving it for publication was Yunlong Cai.

to attain higher DOA tracking accuracy. In [23], DOA Estimation of coherent signals is discussed based on the concept of coprime array interpolation.

Inspired by 1D sparse array design, many two-dimensional (2D) planar sparse arrays (PSAs) have been proposed for virtual URA constructions. 2D nested arrays (2DNA) [24], [25] and 2D coprime arrays (2DCA) [26] are two typical PSAs which are naturally generalized from 1D configurations. Based on the 2D coprime array, recently, the generalized coprime planar array [27] and the corresponding fast search approach [28] have been proposed for computational load reduction. Although the above structures provide higher DOF than the URA, the DOF can still be further improved. Open box array [29] is verified having the largest aperture for the same number of sensors among all the PSAs. However, it suffers severe mutual coupling from the dense sensor locations. To enlarge the adjacent spacings with the virtual URA no change, a series of configurations have been proposed, including partially open box arrays, half open box arrays, half open box arrays with two layers, hourglass arrays [30], half H arrays and ladder arrays [31]. Hence, one can expect that these 2D PSAs could acquire higher number of DOF and have lower mutual coupling.

All the aforementioned works are based on the difference co-array construction. On the other hand, diff-sum co-array (DSCA) have been exploited for underdetermined DOA estimation recent years. The DSCA concept is proposed in [32], which utilizes the vectorized conjugate augmented MUSIC (VCAM) algorithm to construct both sum co-array (SCA) and difference co-array. In [33], a DSCA-based 2DCA is proposed. However, holes in the DSCA still limit the size of its consecutive part. As a result, the performance of subspace-based algorithm is influenced severely. In fact, as the additional SCA information is properly made use of, the DSCA can remedy some holes in DCA and therefore acquire higher DOF than the sparse arrays with only DCA considered.

L-shaped array (LA) [34] is a PSA used for 2D DOA estimation. As its DCA cannot provide large size of URA, there are not many works talking about its use in virtual array construction. In this paper, we exploit the DSCA concept onto the LA to explore its potential in virtual aperture enhancement. Benefit from its special characteristics, the virtual elements in the four quadrants of DSCA have the least redundancy. Therefore, it can acquire the largest virtual aperture with the same number of sensors, compared with the existing PSAs. To further reduce the redundancy of elements on the x and y axes of DSCA, an element moving strategy is proposed. Based on this strategy, any sensor can be relocated to the centrosymmetric positions. Therefore,the generalized L-shaped array (GLA) concept is presented for lower mutual coupling achievement. With the elements selected properly, a new configuration referred to as generalized L-shaped array with odd-even locations (GLA-OEL) is developed. The new geometry is guaranteed to have much lower mutual coupling and higher DOF performance than the existing PSAs. Simulations verify the superiorities of the proposed array with the spatial smoothing ESPRIT algorithm used.

Contributions of this paper are summarized as below:

- The DSCA property of the conventional LA is reconsidered and an element moving strategy is proposed to improve the configuration. The strategy brings generalization to the LA so that the new configurations named as generalized L-shaped array (GLA) can achieve reduced mutual coupling effect with their DSCA remaining intact.
- The optimization configuration among all GLAs referred to as generalized L-shaped array with odd-even locations (GLA-OEL) is developed. By exploiting the lower mutual coupling brought by the element moving strategy and the higher DOF brought by the DSCA property of LA, the GLA-OEL can achieve better performance than other existing PSAs.

The rest of this paper is organized as follows. In Section II, the 2D signal model with and without mutual coupling, the VCAM algorithm and the L-shaped array are reviewed. In Section III, the moving strategy and its use on L-shaped array are proposed. Then, a specific geometry named as GLA-OEL is presented in Section IV. The DOF evaluation, weight functions and aperture analysis are concluded and compared as well. Simulation results are provided and analyzed in Section V. Section VI concludes the paper.

Notations: Denote vectors and matrices by using lower-case and upper-case bold characters, respectively. Double line characters are used to denote sets. Specifically, $(.)^*$ denotes complex conjunction, whereas $(.)^T$ and $(.)^H$ denote the transpose and conjugate transpose of a matrix or vector, respectively. $vec(.)$ implies the vectorization operator which turns a matrix into a column vector. $E(.)$ is the statistical expectation operator. $diag(x)$ denotes a diagonal matrix with the elements of x as the diagonal elements. $\otimes$ and $\odot$ denote Kronecker product and KR product, respectively.

II. PRELIMINARIES

A. SIGNAL MODEL AND VCAM ALGORITHM

Consider an N-elements planar array with physical sensors located at $\mathbb{P} \cdot d = \{\boldsymbol{p}_1, \boldsymbol{p}_2, \cdots, \boldsymbol{p}_N\}d$. Here $\boldsymbol{p}_i = (n_{xi}, n_{yi}) \in \mathbb{Z}^2$ for $i = 1, 2, \cdots, N$ is the position coordinates of the ith sensor. $d = \lambda/2$ is the unit interval between sensors with λ being the wavelength. $\boldsymbol{p}_1 = (0, 0)$ is the reference point. Suppose K far-field narrow-band uncorrelated deterministic signal sources with power of $\delta_k^2, (k = 1, 2, \cdots, K)$ impinging on the array with DOAs as (θ_k, ϕ_k). θ_k and ϕ_k are the azimuth and elevation angles of the kth source. Then, the received signal of the sensor array can be expressed as

$$\boldsymbol{x}(t) = \sum_{k=1}^{K} \boldsymbol{a}(\theta_k, \phi_k)s_k(t) + \boldsymbol{n}(t) = \boldsymbol{A}\boldsymbol{s}(t) + \boldsymbol{n}(t), \qquad (1)$$

where $\boldsymbol{s}(t) = [s_1(t), s_2(t), \cdots, s_K(t)]^T$ is the signal source vector with $s_k(t) = u_k e^{j\omega_k t}$. u_k is the deterministic complex amplitude and ω_k is the base-band signal frequency of the kth signal. $\boldsymbol{n}(t) = [n_1(t), n_2(t), \cdots, n_N(t)]^T$ is

noise vector. The noise is set to be the additive spatially white Gaussian noise with zero mean and variance δ_n^2. $\boldsymbol{A} = [\boldsymbol{a}(\theta_1,\phi_1),\boldsymbol{a}(\theta_2,\phi_2),\cdots,\boldsymbol{a}(\theta_K,\phi_K)]$ is the array manifold matrix, and $\boldsymbol{a}(\theta_k,\phi_k)$ is the steering vector of the kth DOA (θ_k,ϕ_k), given by $\boldsymbol{a}(\theta_k,\phi_k) = [1, e^{j\pi(n_{x_2}cos\theta_k sin\phi_k + n_{y_2}sin\theta_k sin\phi_k)},\cdots, e^{j}\pi(n_{x_N}cos\theta_k sin\phi_k + n_{y_N}sin\theta_k sin\phi_k)]$.

If we consider the mutual coupling, the signal model in Eq. (1) has to be modified as $\boldsymbol{x}(t) = \boldsymbol{CAs}(t) + \boldsymbol{n}(t)$, where $\boldsymbol{C}$ is the mutual coupling matrix. In general, $\boldsymbol{C}$ can be approximated as a B-banded symmetric Toeplitz matrix with the (i,j) element as [30]

$$\boldsymbol{C}_{i,j} = \begin{cases} c_{|\boldsymbol{p}_i - \boldsymbol{p}_j|_{\ell_2}}, & \text{if } |\boldsymbol{p}_i - \boldsymbol{p}_j|_{\ell_2} \le B, \\ 0, & \text{otherwise}, \end{cases} \tag{2}$$

where $\boldsymbol{p}_i, \boldsymbol{p}_j \in \mathbb{P}$ and $|\boldsymbol{p}_i - \boldsymbol{p}_j|_{\ell_2}$ denotes the distance between the two points. The coupling coefficients satisfy $1 = c_0 > |c_1| > |c_{\sqrt{2}}| > \cdots > |c_B|$. In this paper, we assume that $c_0 = 1$ and $c_l = c_1 e^{-j(l-1)\pi/8}/l$ if $l \le B$.

Then,we introduce the VCAM algorithm in [32]. First, collect N_s snapshots of $x_1(t)$ and $x_i(t)$ with delay $\tau \ne 0$ and obtain $[x_1(1), x_1(2),\cdots,x_1(N_s)]$, $[x_i(1+\tau), x_i(2+\tau),\cdots,x_i(N_s+\tau)]$. Then, calculating the time average function of $x_1^*(t)$ and $x_i(t+\tau)$. Note that the signals and noise are uncorrelated, one has

$$\begin{aligned} &R_{x_1^* x_i}(\tau) \\ &= 1/N_s \sum_{t=1}^{N_s} x_1^*(t) x_i(t+\tau) \\ &= 1/N_s \sum_{t=1}^{N_s} [\sum_{k=1}^{K}\sum_{l=1}^{K} a_{k,1}^* a_{l,i} s_k^*(t) s_l(t+\tau) + n_l^*(t) n_k(t+\tau) \\ &\quad + \sum_{k=1}^{K} a_{k,1}^* s_k^*(t) n_i(t+\tau) + \sum_{l=1}^{K} a_{l,i}^* s_l^*(t+\tau) n_l(t)]. \\ &\approx \sum_{k=1}^{K}\sum_{l=1}^{K} a_{k,1}^* a_{l,i} R_{s_k^* s_l}(\tau) R_{n_k^* n_l}(\tau) \end{aligned} \tag{3}$$

where $a_{k,1}^* = 1$, $R_{s_k^* s_l}(\tau) = \sum_{t=1}^{N_s} s_k^*(t) s_l(t+\tau)/N_s = u_k^* u_l e^{j\omega_l \tau} \sum_{t=1}^{N_s} e^{j(\omega_l - \omega_k)t}/N_s$ and $R_{n_k^* n_l}(\tau) = \sum_{t=1}^{N_s} n_1^*(t) n_i(t+\tau)/N_s$. Assume $k \ne l$ and N_s is sufficiently large. Then, $\sum_{t=1}^{N_s} e^{j(\omega_l - \omega_k)t}/N_s \approx 0$. Moreover, $R_{n_1^* n_i}(\tau) \approx 0$ as $n_i(t)$ is zero-mean white Gaussian noise.

Based on the above fact, the time average function can be further simplified as $R_{x_1^* x_i}(\tau) = \sum_{k=1}^{K} a_{k,i} R_{s_k^* s_k}(\tau)$, where $R_{s_k^* s_k}(\tau) \approx \sum_{t=1}^{N_s} s_k^*(t) s_k(t+\tau)$. Obviously, $R_{s_k^* s_k}(\tau)$ can be viewed as an equivalent source signal with the power of δ_k^4. By stacking all the vectors $R_{x_1^* x_i}(\tau)$, one has

$$\boldsymbol{v}_{xx}(\tau) = \boldsymbol{A}\boldsymbol{v}_{ss}(\tau), \tag{4}$$

where $\boldsymbol{v}_{xx}(\tau) = [R_{x_1^* x_1}(\tau), R_{x_1^* x_2}(\tau),\cdots,R_{x_1^* x_N}(\tau)]^T$ and $\boldsymbol{v}_{ss}(\tau) = [R_{s_1^* s_1}(\tau),\cdots,R_{s_K^* s_K}(\tau)]^T$. If we invert τ to $-\tau$ and take the conjugate, Eq. (4) becomes

$$[\boldsymbol{v}_{xx}(-\tau)]^* = \boldsymbol{A}^* \boldsymbol{v}_{ss}(\tau), \tag{5}$$

With Eq. (4) and (5) combined together, the conjugate augmented correlation vector has the form of

$$\boldsymbol{y}(\tau) = \begin{bmatrix} [\boldsymbol{v}_{xx}(-\tau)]^* \\ \boldsymbol{v}_{xx}(\tau) \end{bmatrix} = \bar{\boldsymbol{A}}\boldsymbol{v}_{ss}(\tau), \tag{6}$$

where $\bar{\boldsymbol{A}} = [\boldsymbol{A}^*, \boldsymbol{A}^T]^T = [\bar{\boldsymbol{a}}_1,\cdots,\bar{\boldsymbol{a}}_k,\cdots,\bar{\boldsymbol{a}}_K]$ with $\bar{\boldsymbol{a}}_k = [\boldsymbol{a}_k^H, \boldsymbol{a}_k^T]^T$.

Suppose the pseudo snapshots and pseudo sampling interval as N_{sp} and τ_p. Then, the pseudo-data matrix is $\boldsymbol{R}_{yy} = [\boldsymbol{y}(\tau_p),\cdots,\boldsymbol{y}(\tau_p N_{sp})] = \bar{\boldsymbol{A}}\boldsymbol{R}_{ss}\bar{\boldsymbol{A}}^H$, where $\boldsymbol{R}_{ss} = diag([\delta_1^4,\cdots,\delta_K^4])$ if N_s is sufficiently large.

Vectorizing $\boldsymbol{R}_{yy}$ yields $\boldsymbol{z} = vec(\boldsymbol{R}_{yy}) = (\bar{\boldsymbol{A}}^* \odot \bar{\boldsymbol{A}})\bar{\boldsymbol{s}}$, where $\bar{\boldsymbol{s}} = [\delta_1^4, \delta_2^4,\cdots,\delta_K^4]$. Note that $\bar{\boldsymbol{s}}$ can now be viewed as virtual input signal source and the jth column of $\bar{\boldsymbol{A}}^* \odot \bar{\boldsymbol{A}}$ has the form of

$$\bar{\boldsymbol{a}}_j^* \otimes \bar{\boldsymbol{a}}_j = \begin{bmatrix} \boldsymbol{a}_j^* \\ \boldsymbol{a}_j \end{bmatrix}^* \otimes \begin{bmatrix} \boldsymbol{a}_j^* \\ \boldsymbol{a}_j \end{bmatrix} = \begin{bmatrix} \boldsymbol{a}_j \otimes \begin{bmatrix} \boldsymbol{a}_j^* \\ \boldsymbol{a}_j \end{bmatrix} \\ \boldsymbol{a}_j^* \otimes \begin{bmatrix} \boldsymbol{a}_j^* \\ \boldsymbol{a}_j \end{bmatrix} \end{bmatrix}. \tag{7}$$

It can be seen that $\boldsymbol{z}$ can be viewed as an equivalent signal vector received from the sum co-array and difference co-array. We call the combination of SCA and DCA as the diff-sum co-array in this paper. Their definitions are given below.

Definition 1: For a 2D planar array specified by $\mathbb{P}$, one can define the following co-arrays

$$\begin{cases} \textbf{Sum co-array (SCA):} \mathbb{S} = \{\pm(\boldsymbol{p}_j + \boldsymbol{p}_i) | \boldsymbol{p}_j, \boldsymbol{p}_i \in \mathbb{P}\}; \\ \textbf{difference co-array (DCA):} \\ \mathbb{D} = \{(\boldsymbol{p}_j - \boldsymbol{p}_i) | \boldsymbol{p}_j, \boldsymbol{p}_i \in \mathbb{P}\}; \\ \textbf{Diff-sum Co-array (DSCA):} \\ \mathbb{DS} = \mathbb{D} \cup \mathbb{S} = \{\pm(\boldsymbol{p}_j + \boldsymbol{p}_i) \cup (\boldsymbol{p}_j - \boldsymbol{p}_i) | \boldsymbol{p}_j, \boldsymbol{p}_i \in \mathbb{P}\}; \end{cases} \tag{8}$$

Assume a virtual URA of size $(2L_{ux}+1)\times(2L_{uy}+1)$ exists in $\mathbb{DS}$. Extracting the corresponding elements from $\boldsymbol{z}$, rearranging them and taking the average of the repeated entries, one can obtain the equivalent covariance matrix

$$\boldsymbol{R}_{zz} = \frac{1}{(L_{ux}+1)(L_{uy}+1)} \sum_{i=1}^{L_{ux}+1}\sum_{j=1}^{L_{uy}+1} \tilde{\boldsymbol{z}}_{i,j}\tilde{\boldsymbol{z}}_{i,j}^H \tag{9}$$

where $\tilde{\boldsymbol{z}}_{i,j} = \tilde{\boldsymbol{A}}\bar{\boldsymbol{s}}$ is the output of the URA whose sensors locating at $[-i+1, -i+1+L_{ux}]\times[-j+1, -j+1+L_{uy}]$, for $i = 1,\cdots,L_{ux}+1$ and $j = 1,\cdots,L_{uy}+1$. $\tilde{\boldsymbol{A}}$ is a $(1+L_{ux})(1+L_{uy})\times K$ matrix and can be treated as the array manifold of such URA.

Apply 2D DOA algorithms such as Unitary-ESPRIT [35] on $\boldsymbol{R}_{zz}$. Then, one can estimate the 2D DOAs successfully.

B. L-SHAPED ARRAY AND ITS DSCA PROPERTIES

In this subsection, we will review the LA first and then deduce the DSCA and DOF properties. L-shaped array consists of two dense sub-ULAs on the positive axes, which is defined by

Definition 2 (L-Shaped Array [36], LA): For two positive integers N_x, N_y, L-shaped array is characterized by integer sets

$$\mathbb{P}_{LA} = \mathbb{H} \cup \mathbb{V}, \tag{10}$$

where $\mathbb{H} = \{(n_x, 0)|n_x \in \{0, 1, \ldots, N_x\}\}$ and $\mathbb{V} = \{(0, n_y)|n_y \in \{0, 1, \ldots, N_y\}\}$.

If we conduct the VCAM algorithm, then a diff-sum virtual array will be generated. To see the DSCA more clearly, properties like degrees of freedom and weight function are defined and provided.

Definition 3 (Degrees of Freedom): Denote $\mathbb{U}$ as the largest URA in the DSCA of a specific 2D planar array $\mathbb{P}$. The number of degrees of freedom is the cardinality of $\mathbb{U}$.

Definition 4 (Weight Function): For a 2D array specified by $\mathbb{P}$, assume the difference co-array is $\mathbb{D}$. The weight function is the number of sensor pairs with separation $\vec{l} \in \mathbb{D}$, i.e.,

$$\omega(\vec{l}) = \langle\{(\boldsymbol{p}_i, \boldsymbol{p}_j)|\boldsymbol{p}_i, \boldsymbol{p}_j \in \mathbb{P}, \boldsymbol{p}_i - \boldsymbol{p}_j = \vec{l}\}\rangle, \tag{11}$$

where $\langle\cdot\rangle$ denotes the number of elements inside.

It should be noted that the weight function here is the number of sensor pairs with distance $\vec{l}$ but not the pairs generating the co-array index $\vec{l}$. Therefore, $\vec{l} \in \mathbb{D}$ but $\vec{l} \notin \mathbb{S}$. Then we have Property 1.

Property 1: For positive integers N_x and N_y, LA defined in Eq. (10) has the largest virtual URA in DSCA located at

$$\mathbb{U}_{LA} = \{(n_x, n_y)| - N_x \le n_x \le N_x, -N_y \le n_y \le N_y\}. \tag{12}$$

The DOF of LA is $(2N_x+1)\times(2N_y+1)$. The weight function can be expressed as

$$w(1,0)=N_x,\ \ w(0,1)=N_y,\ \ w(1,1)=0,\ \ w(-1,1)=1. \tag{13}$$

The proof of Property 1 is provided in the Appendix A. As shown in Fig. 1(a), no sensor pairs with separations $\vec{l} = (1, 1), (-1, -1)$ exist since both of the sub-ULAs locate at the positive axes. Therefore, $w(1, 1) = w(-1, -1) = 0$. Besides, as can be seen from Fig. 1(b), with only $N = N_x + N_y + 1$ physical sensors, a virtual URA of size $(2N_x + 1) \times (2N_y + 1)$ is obtained. As a contrast, the existing optimal 2D PSA OBA has to make use of N_x+2N_y+1 sensors to get the same size of virtual URA by utilizing the DCA concept. Therefore, applying the VCAM onto LA increases the number of DOF with the same number of sensors. From the property mentioned above, we find that the weight function $w(1, 0)$ and $w(0, 1)$ are quite large due to the dense ULA on the axes. To decrease the mutual coupling, we propose the following generalized L-shaped array concept.

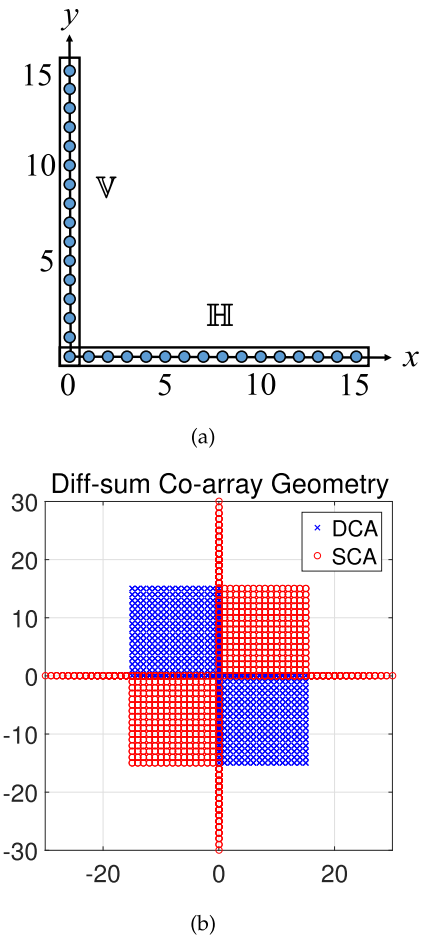

FIGURE 1. (a) The L-shaped array with $N_x = 15$ and $N_y = 15$. The blue dots are physical sensors. (b) The DSCA of the above LA. The blue crosses represent difference co-array elements. The red dots are sum co-array elements.

III. GENERALIZED L-SHAPED ARRAY CONCEPT

The dense distribution of sensors on both axes in LA arises the strong interference between the adjacent elements. If we can relocate some of these sensors and guarantee the largest URA in the DSCA with no change, it is possible to reduce the weight functions $w(1, 0)$ and $w(0, 1)$. Therefore, how to choose the elements and where to relocate them are the most important problems we will resolve.

Let $\mathbb{P}$ be the location set of an arbitrary PSA and let $\mathbb{DS}$ be the corresponding DSCA. Choose Q sensors located at $(n_{xq}, n_{yq}) \in \mathbb{P}$ for $q = 1, 2, \ldots, Q$ and relocate them to $(\widehat{n}_{xq}, \widehat{n}_{yq}) \notin \mathbb{P}$. As such, a new PSA denoted as $\widehat{\mathbb{P}}$ is generated with its DSCA being $\widehat{\mathbb{DS}}$. The follow lemma provides us an effective moving strategy to keep the DSCA invariant.

Lemma 1: $\widehat{\mathbb{DS}} = \mathbb{DS}$ if $(\widehat{n}_{xq}, \widehat{n}_{yq}) = -(n_{xq}, n_{yq})$ for $q = 1, 2, \ldots, Q$.

The proof is provided in the Appendix B. Lemma 1 indicates that any physical sensors in a PSA can be moved with the DSCA invariant, as long as they are relocated at the centrosymmetric positions. As an example, Fig. 2 illustrates a PSA with only two sensors at position A and B. Vector $\boldsymbol{l}_{AB}$, $\boldsymbol{l}_{BA}$ and $\boldsymbol{l}_{OC}$, $\boldsymbol{l}_{OC'}$ form the DCA and SCA of the DSCA,

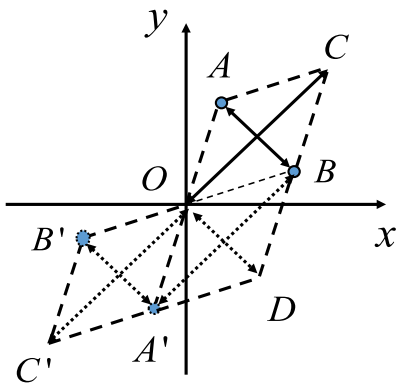

FIGURE 2. An example of moving strategy. *A* and *B* are original locations. *A′* and *B′* are the centrosymmetric positions of *A* and *B*.

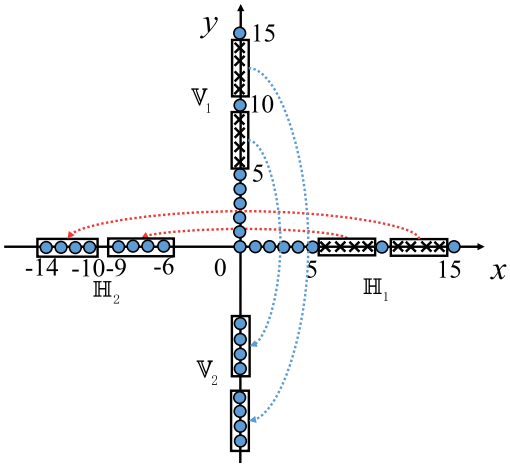

FIGURE 3. A GLA with $N_x = 15$ and $N_y = 15$. $\mathbb{H}_1$ and $\mathbb{H}_2$ are nested arrays.

respectively. If element A is moved to its centrosymmetric location A', then $\boldsymbol{l}_{A'B} = \boldsymbol{l}_{OC}$ and $\boldsymbol{l}_{BA'} = \boldsymbol{l}_{OC'}$ generate the new DCA, which is in fact the SCA of the original PSA. At the same time, $\boldsymbol{l}_{OD} = \boldsymbol{l}_{AB}$ and $\boldsymbol{l}_{OD'} = \boldsymbol{l}_{BA}$ form the new SCA, which is the same as the original DCA. Therefore, we have $\mathbb{DS} = \widehat{\mathbb{DS}}$. If both sensors are moved to A' and B' simultaneously, $\widehat{\mathbb{DS}}$ will be the mirror structure of $\mathbb{DS}$.

Lemma 1 provides the basic idea for sensor redistribution. Applying this strategy on the LA, then we can obtain the following generalized L-shaped array concept.

Definition 5 (Generalized L-Shaped Array, GLA) For positive integers N_x and N_y, generalized L-shaped array is defined as a PSA located at

$$\mathbb{P}_{GLA} = \mathbb{H}_1 \cup \mathbb{H}_2 \cup \mathbb{V}_1 \cup \mathbb{V}_2, \tag{14}$$

where $\mathbb{H}_1 = \{(n_x, 0)|n_x \geq 0, n_x \in h_1\}$, $\mathbb{H}_2 = \{(n_x, 0)|n_x < 0, n_x \in h_2\}$, $\mathbb{V}_1 = \{(0, n_y)|n_y \geq 0, n_y \in v_1\}$ and $\mathbb{V}_2 = \{(0, n_y)|n_y < 0, n_y \in v_2\}$, satisfying

1) $h_1 \cup (-h_2) = \{0, 1, 2, \ldots, N_x\}$, $v_1 \cup (-v_2) = \{0, 1, 2, \ldots, N_y\}$;

2) $h_1 \cap (-h_2) = \emptyset$, $v_1 \cup (-v_2) = \emptyset$ with $\emptyset$ being the empty set.

Fig. 3 depicts an example of GLA with $N_x = 15$ and $N_y = 15$. In this case, h_1 and v_1 are 1D nested arrays [7] with elements located at $\{0, 1, 2, 3, 4, 5, 10, 15\}$. $h_2 = v_2 = \{-6, -7, -8, -9, -11, -12, -13, -14\}$ are the 1D sparse arrays with elements moved from $\{6, 7, 8, 9, 11, 12, 13, 14\}$ to their centrosymmetric positions. Therefore, for GLA, the subsets h_1, h_2, v_1 and v_2 satisfy Lemma 1. It has the same DSCA as the original LA. Furthermore, due to the distributive locations in GLA, its separations of $w(1, 0)$ and $w(0, 1)$ will be dramatically reduced. With the subarrays in GLA properly designed, lower mutual coupling can be achieved. Note that the subarrays can be any 1D array configurations. LA is a special case of GLA with $h_1 = \{0, 1, 2, \ldots, N_x\}$, $v_1 = \{0, 1, 2, \ldots, N_y\}$ and h_2, v_2 being empty sets.

Property 2: For positive integers N_x and N_y, GLA defined in Eq. (14) has the same DSCA with the LA in Eq. (10). The DOF is $(2N_x + 1) \times (2N_y + 1)$.

Proof: As $h_1 \cup (-h_2) = \{0, 1, 2, \ldots, N_x\}$ and h_2, $-h_2$ are centrosymmetric to each other, we conclude that GLA is a LA with part of the elements at $-\mathbb{H}_2$ moved to their centrosymmetric positions. Similar conclusion can be obtained for v_1 and $-v_2$. According to Lemma 1, we have $\mathbb{DS}_{GLA} = \mathbb{DS}_{LA}$. Therefore, the largest virtual URA in the DSCA of GLA locates at set $\mathbb{U}_{LA} = \{(n_x, n_y)| - N_x \leq n_x \leq N_x, -N_y \leq n_y \leq N_y\}$. The number of DOF is the size of the virtual URA, i.e., $(2N_x + 1) \times (2N_y + 1)$. □

IV. GENERALIZED L-SHAPED ARRAY WITH ODD-EVEN LOCATIONS

A. GENERALIZED L-SHAPED ARRAY WITH ODD-EVEN LOCATIONS

Under the framework of GLA, there are many potential geometries. In this subsection, we will propose a special GLA, named as Generalized L-shaped array with odd-even locations (GLA-OEL), which possesses the lowest mutual coupling effect with each 2D separation.

Definition 6: (Generalized L-Shaped Array With Odd-Even Locations, GLA-OEL) For positive integers N_x and N_y, generalized L-shaped array with odd-even locations is a generalized L-shaped array defined by Eq. (14) with

$$\begin{cases} h_1 = \{0, 1 + 2\ell \mid 0 \leq \ell \leq \lfloor \dfrac{N_x - 1}{2} \rfloor\} \\ h_2 = \{-2\ell \mid 1 \leq \ell \leq \lfloor \dfrac{N_x}{2} \rfloor\} \\ v_1 = \{0, 1 + 2\ell \mid 0 \leq \ell \leq \lfloor \dfrac{N_y - 1}{2} \rfloor\} \\ v_2 = \{-2\ell \mid 1 \leq \ell \leq \lfloor \dfrac{N_y}{2} \rfloor\}. \end{cases} \tag{15}$$

Fig. 4 illustrates an example of GLA-OEL with $N_x = 15$ and $N_y = 15$. It can be observed that except the 0 point, all the subsets on the positive or negative part of the GLA-OEL are ULAs with separation 2. The positive axes are two odd sequences with $h_1 = v_1 = \{0, 1, 3, 5, 7, 9, 11, 13, 15\}$. While the negative parts are two even sequence sets with $h_2 = v_2 = \{-2, -4, -6, -8, -10, -12, -14\}$. Meanwhile,

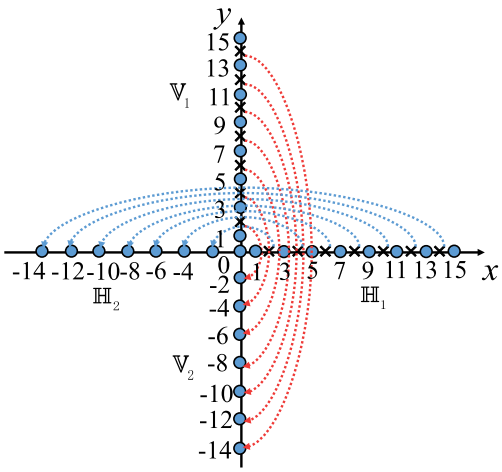

FIGURE 4. A GLA-OEL with $N_x = 15$ and $N_y = 15$. $\mathbb{H}_1 = \mathbb{V}_1 = \{0, 1, 3, 5, 7, 9, 11, 13, 15\}$. $\mathbb{H}_2 = \mathbb{V}_2 = \{-2, -4, -6, -8, -10, -12, -14\}$.

$h_1 \cup (-h_2) = v_1 \cup (-v_2) = \{0, 1, \ldots, 15\}$. The number of sensors is $N = N_x + N_y + 1 = 31$.

As the GLA-OEL is a special instance of GLA, it has the same properties in Property 1. In addition, there is only one sensor pair (1, 0), (0, 0) contribute to $w(1, 0)$. Therefore, $w(1, 0) = 1$. Similarly, in the vertical direction, only the pair (0, 1), (0, 0) generates the $w(0, 1)$. While the separation $\vec{l} = (1, -1)$ is generated by (1, 0), (0, 1). There is no sensors having the difference $\vec{l} = (1, 1)$. As a result, the following property of GLA-OEL can be deduced.

Property 3: For two positive integers N_x and N_y, GLA-OEL defined in Eq. (15) has the same DCSA as LA with the DOF being $(2N_x + 1) \times (2N_y + 1)$. It has much less sensor pairs with small separations than LA. The weight functions can be expressed as $w(0, 1) = 1$, $w(1, 0) = 1$, $w(1, 1) = 0$ and $w(1, -1) = 1$.

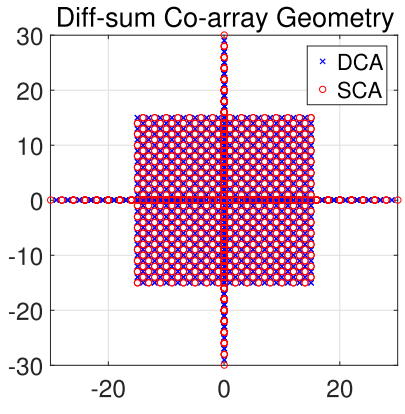

FIGURE 5. The DSCA of the GLA-OEL with $N_x = 15$ and $N_y = 15$. The blue crosses are the DCA elements. The red dots are the SCA elements.

Fig. 5 illustrates the DSCA of the GLA-OEL. Compared with Fig. 1 (b), the new geometry has the same virtual DSCA as that of the original LSA with only the specific distribution of sum results and difference results different, which coincides with the moving strategy in Lemma 1.

B. COMPARISONS

In this subsection, a series of 2D array configurations, such as 2D nested array (2DNA) [24], half open box array with two layers (HOBA-2), hourglass array (HA) [30], and Laddar Array (LdA) [31], which make use of the DCA to acquire virtual aperture, are compared with three DSCA based PSAs, i.e., 2D coprime array (2DCA) [33], L-shaped array and GLA-OEL proposed in this paper.

1) DEGREE OF FREEDOM

For both LA and GLA-OEL, $N_x + 1$ physical sensors are supposed to locate on the x-axis. In the vertical direction, $N_y + 1$ sensors are positioned. With (0, 0) as the common point of the two axes, the total number of sensors is $N = N_x + N_y + 1$. As provided in Property 1 and 3, the largest URA in the DSCA has the size of

$$\mathrm{DOF}_{LA} = \mathrm{DOF}_{GLA-OEL} = (2N_x + 1)(2N_y + 1). \quad (16)$$

For 2DNA, configuration II in [25] is considered which possesses higher DOF than configuration I. The geometry we use for comparison has two URAs inside. One is a dense square with $N_x \times N_x$ elements separating unit spacings. Another one is a sparse square with $N_y \times N_y$ elements separating N_x unit spacings. The total number of sensors is $N = N_x^2 + N_y^2 - 1$. The number of DOF generated by DCA is

$$\mathrm{DOF}_{2DNA} = (2N_xN_y - 1)N_xN_y. \quad (17)$$

For 2DCA, suppose two coprime parameters N_x and N_y. $(N_x > N_y)$ The geometry has two URAs inside. One is a square with $N_x \times N_x$ elements separating N_y unit spacings. Another one is a square with $2N_y \times 2N_y$ elements separating N_x unit spacings. The total number of sensors is $N = N_x^2 + N_y^2 - 1$. The number of DOF generated by its virtual array is

$$\mathrm{DOF}_{2DCA} = (N_xN_y + N_x + N_y - 1)^2. \quad (18)$$

For HOBA-2, HA and LdA, suppose N_x sensors are located at the horizontal direction. $2N_y - 2$ sensors distribute on the vertical lines. The total number of sensors is $N = N_x + 2N_y - 2$. Then, the DCA is proved to be a hole-free URA with the size of

$$\begin{aligned}\mathrm{DOF}_{HOBA-2} &= \mathrm{DOF}_{HA} \\ &= \mathrm{DOF}_{LdA} = (2N_x - 1)(2N_y - 1). \quad (19)\end{aligned}$$

The DOF comparisons of the seven PSAs are presented in Table 1. For 2DNA, HOBA-2, HA, LdA, LA and GLA-OEL, $N = 49$. Since 2DCA fail to have examples for $N = 49$, N is approximately set to be 51. The optimal parameters are used for each PSA. As can be seen, LA and GLA-OEL can achieve the highest number of DOF among all the structures. HOBA-2, HA, LdA and 2DNA can only provide the half number. Furthermore, 2DCA achieves the least number of DOF with 2 more sensors because of the holes in its DSCA. The reason is that LA-like arrays have the lowest redundancy in the DCSA generations. Therefore, with the same number of sensors utilized, more sources can be detected.

TABLE 1. DOF of different PSAs.

Array Structures	Array Parameters (N_x, N_y)	DOF
$2DCA^{\dagger}_{DSCA}$	$(4,3)$	324
$2DNA_{diff}$	$(5,5)$	1225
$HOBA\text{-}2_{diff}$	$(25,13)$	1225
HA_{diff}	$(25,13)$	1225
LdA_{diff}	$(25,13)$	1225
LA_{DSCA}	$(24,24)$	2401
$GLA\text{-}OEL_{DSCA}$	$(24,24)$	2401

† For 2DCA, $N = 51$ while for the other configurations, $N = 49$.

2) WEIGHT FUNCTIONS

For LA, as given in Property 1, the weight functions can be expressed as

$$w(1,0) = N_x, \quad w(0,1) = N_y, \; w(1,1) = 0, \; w(-1,1) = 1.$$

For GLA-OEL, as indicated by Property 3, the weight functions are

$$w(0,1) = 1, \quad w(1,0) = 1, \; w(1,1) = 0, \; w(1,-1) = 1.$$

For 2DNA, the weight functions are [25]

$$w(0,1) = N_x(N_x-1), \quad w(1,0) = N_x(N_x-1),$$
$$w(1,1) = w(1,-1) = (N_x-1)^2.$$

For HOBA-2, the weight functions can be expressed as [30]

$$w(0,1) = \begin{cases} 4, & \text{if } N_y \text{ is odd} \\ 6, & \text{if } N_y \text{ is even} \end{cases}, \quad w(1,0) = 2,$$

$$w(1,1) = w(1,-1) = \begin{cases} N_y - 2, & \text{if } N_y \text{ is odd} \\ N_y - 3, & \text{if } N_y \text{ is even.} \end{cases}$$

For HA, the weight functions can be expressed as [30]

$$w(0,1) = \begin{cases} 8, & \text{if } N_y \text{ is odd} \\ 10, & \text{if } N_y \text{ is even} \end{cases}, \quad w(1,0) = 2,$$

$$w(1,1) = w(1,-1) = \begin{cases} 3, & \text{if } N_y = 7, 8 \\ 5, & \text{if } N_y = 10 \text{ or } 2r+1, \; r \geq 4 \\ 7, & \text{if } N_y = 4r, \; r \geq 3 \\ 9, & \text{if } N_y = 4r+2, \; r \geq 3 \end{cases}$$

For LdA, the weight functions are

$$w(0,1) = \begin{cases} 8, & \text{if } N_y \text{ is odd} \\ 10, & \text{if } N_y \text{ is even} \end{cases}, \quad w(1,0) = 2,$$

$$w(1,1) = w(1,-1) = \begin{cases} 3, & \text{if } N_y = 7, 8 \\ 5, & \text{if } N_y = 10 \text{ or } 2r+1, \; r \geq 4 \\ 7, & \text{if } N_y = 4r, \; r \geq 3 \\ 9, & \text{if } N_y = 4r+2, \; r \geq 3 \end{cases}.$$

For 2DCA, its weight functions depend on its coprime parameters N_x and N_y. However, the specific weight functions with $N = 51, N_x = 4, N_y = 3$ are still compared below.

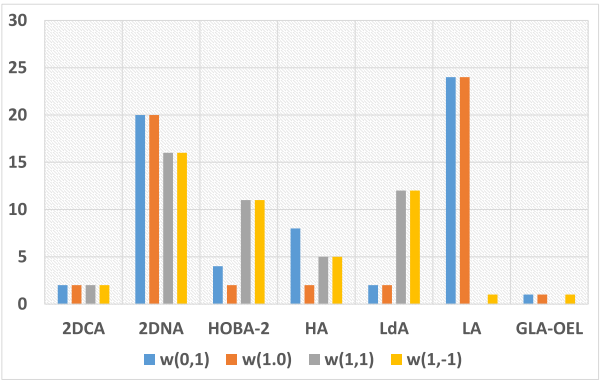

FIGURE 6. Comparisons of weight functions.

To take clear insight into the mutual couplings, an example with $N = 49$ is illustrated in TABLE 2 and Figure 6. It can be concluded that no matter in which direction, GLA-OEL can achieve the smallest weight function. Therefore, it performs better than any other PSAs when mutual couplings between adjacent sensors exist. It is the application of DSCA concept and the special characteristic of GLA-OEL that provide the superiority.

TABLE 2. Comparisons of weight functions.

Array Structures (N_x, N_y)	w(0,1)	w(1,0)	w(1,1)	w(1,-1)
$2DCA^{\dagger}$ $(4,3)$	2	2	2	2
2DNA $(5,5)$	20	20	16	16
HOBA-2 $(25,13)$	4	2	11	11
HA $(25,13)$	8	2	5	5
LdA $(25,13)$	2	2	12	12
LA $(24,24)$	24	24	0	1
GLA-OEL $(24,24)$	1	1	0	1

† For 2DCA, $N = 51$ while for the other configurations, $N = 49$.

3) APERTURE

Definition 7 (Array Aperture) Suppose a PSA $\mathbb{P}$, where $\mathbb{P} = \{(x,y)|\forall x \in [x_-, x_+], \forall y \in [y_-, y_+]\}$ with x_-, x_+, y_-, y_+ are arbitrary integers. Then the aperture of a PSA has two dimensions. Define them as x-aperture and y-aperture, which denote as $\mathbb{A}_x$ and $\mathbb{A}_y$, respectively. Then $\mathbb{A}_x = x_+ - x_-$' and '$\mathbb{A}_y = y_+ - y_-$'. The array deployment area $\mathbb{A} = \mathbb{A}_x \times \mathbb{A}_y$.

For our proposed array, $\mathbb{A}_x = 2N_x$ and $\mathbb{A}_y = 2N_y$. Therefore, such array needs an area of $\mathbb{A}_x \times \mathbb{A}_y = 4N_xN_y$ to deploy.

For LA, $\mathbb{A}_x = N_x + 1$ and $\mathbb{A}_y = N_y + 1$. The deployment area needed is $\mathbb{A}_x \times \mathbb{A}_y = (N_x+1)(N_y+1)$.

For HOBA-2 and HA $\mathbb{A}_x = N_x$ and $\mathbb{A}_y = N_y$. The area needed for array deployment is $\mathbb{A}_x \times \mathbb{A}_y = N_xN_y$.

For LdA, $\mathbb{A}_x = N_x$ and $\mathbb{A}_y = 2N_y - 2$. The area needed for array deployment is $\mathbb{A}_x \times \mathbb{A}_y = N_x(2N_y - 2)$.

(a) 2DNA, RMSE=0.0757 (b) HA, RMSE=0.0426 (c) LA, RMSE=0.0042

(d) LA, RMSE=0.0013 (e) GLA-OEL, RMSE=0.0012 (f) GLA-OEL, RMSE=0.0003

FIGURE 7. The DOA estimations (∘) and the true directions (×) for different PSAs with the same $N = 49$. (a) 2DNA ($N_x = N_y = 5$) with mutual coupling; (b) HA ($N_x = 25, N_y = 13$) with mutual coupling; (c) LA ($N_x = 24, N_y = 24$) with mutual coupling; (d) LA ($N_x = 24, N_y = 24$) without mutual coupling; (e) GLA-OEL ($N_x = 24, N_y = 24$) with mutual coupling; (f) GLA-OEL ($N_x = 24, N_y = 24$) without mutual coupling. $B = 2$, $c_1 = 0.6$. The SNR=10 dB. The number of pseudo snapshots and snapshots are 100.

For 2DNA, the x-aperture and y-aperture are $\mathbb{A}_x = (N_y - 1)N_x + 1$ and $\mathbb{A}_y = N_y N_x$, respectively. Then the area needed for the array is $\mathbb{A}_x \times \mathbb{A}_y = N_y N_x[(N_y - 1)N_x + 1]$.

For 2DCA, the aperture is also influenced by two coprime parameters N_x and N_y ($N_x > N_y$), which are defined in the previous subsection. Then $\mathbb{A}_x = \mathbb{A}_y = N_x(2N_y - 1) + 1$ and the area of 2DCA is $\mathbb{A}_x \times \mathbb{A}_y = [N_x(2N_y - 1) + 1]^2$.

An example of the deployment area is illustrated in TABLE 3. The proposed GLA-OEL requires the largest array deployment area, which greatly increase the DOF. However, although the aperture is large, the sensors of GLA-OEL are only positioned at x and y axis instead of occupying the whole area.

TABLE 3. Deployment area of different PSAs.

Array Structures	Array Parameters (N_x, N_y)	Array Deployment Area
$2DCA^{\dagger}_{DSCA}$	$(4,3)$	441
$2DNA_{diff}$	$(5,5)$	525
$HOBA\text{-}2_{diff}$	$(25,13)$	325
HA_{diff}	$(25,13)$	325
LdA_{diff}	$(25,13)$	600
LA_{DSCA}	$(24,24)$	625
$GLA\text{-}OEL_{DSCA}$	$(24,24)$	2304

† For 2DCA, $N = 51$ while for the other configurations, $N = 49$.

V. NUMERICAL SIMULATIONS

In this section, we will conduct numerical simulations to demonstrate the superiority of the DSCA construction and low mutual coupling influence in GLA-OEL. Consider $K = 14$ uncorrelated sources with the normalized directions distributing at set $\Theta = \{(\bar{\theta}_k, \bar{\phi}_k)|k = 1, \ldots, K\}$ with $\bar{\theta}_k = sin\theta_k cos\phi_k$, $\bar{\phi}_k = sin\theta_k sin\phi_k$. The normalized directions are defined as $(-0.3, -0.1)$, $(-0.3, 0.1)$, $(-0.3, 0.3)$, $(-0.1, -0.3)$, $(-0.223, -0.223)$, $(-0.1, 0.1)$, $(-0.045, 0.134)$, $(-0.1, 0.3)$, $(0.1, 0.1)$, $(0.1, -0.1)$, $(0.1, 0.3)$, $(0.3, -0.3)$, $(0.3, -0.1)$, $(0.3, 0.1)$. Choose the optimal parameters and number of sensors for all compared configuration as the values in Table 1. The root mean square error (RMSE) has the form of

$$\text{RMSE} = \sqrt{(1/(\tilde{N}K)\sum_{k=1}^{K}\sum_{n=1}^{\tilde{N}}(\hat{\bar{\theta}}_{kn} - \bar{\theta}_{kn})^2 + (\hat{\bar{\phi}}_{kn} - \bar{\phi}_{kn})^2}, \tag{20}$$

where $(\hat{\bar{\theta}}, \hat{\bar{\phi}})$ and $(\bar{\theta}, \bar{\phi})$ are the estimated and true DOAs, respectively; $\tilde{N}$ is the number of independent Monte-Carlo trials.

A. DOA ESTIMATIONS

We assume that the number of pseudo snapshots and snapshots is $N_s = N_{sp} = 100$ and the signal-to-noise ratio (SNR) is 10 dB. Applying the spatial smoothing [9] and unitary ESPRIT algorithm [35] on 2DNA, HA, LA and GLA-OEL, the DOA estimation results are illustrated in Fig. 7. As can be seen, with mutual coupling considered by setting $B = 2$ and $c_1 = 0.6$, Fig. 7(a), (b), (c), (e) shows that the 2DNA and HA fail to estimate some DOAs with the RMSE being 0.0757 and 0.0426. While LA and GLA-OEL can get accurate estimations with RMSE being 0.0042 and 0.0012. The GLA-OEL is capable of estimating the DOA more satisfactorily than any other PSAs. Without mutual coupling effect, as shown in Fig. 7(d) and (f), the estimation results are much better than the case when the couplings exist.

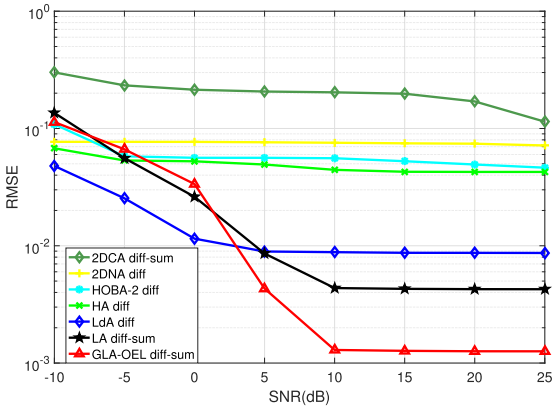

FIGURE 8. RMSE v.s. SNR with $B = 2$, $c_1 = 0.6$. The number of pseudo snapshots and snapshots are $N_{sp} = N_s = 100$.

B. RMSE

The root-mean-square error (RMSE) results obtained at different SNRs varying from -10 dB to 25 dB with pseudo snapshots and snapshots $N_s = N_{sp} = 100$ are illustrated in Fig. 8. 300 independent Monte-Carlo trials are conducted. The parameters for PSAs and the mutual coefficients are the same as that in the first experiment and Table 1. As shown, the GLA-OEL can acquire the lowest RMSE when the SNR is larger than 0 dB. The LA performs better than HOBA-2, HA, 2DNA and 2DCA but a little bit worse than GLA-OEL. Meanwhile, 2DCA achieves the worst resolution even with two more sensors due to its limited DOF. The reason why HOBA-2, HA, 2DNA get lower errors when the SNR is less than -5 dB is that the weight functions of $w(1, 1)$ and $w(1, -1)$ for LA and GLA-OEL are much lower than the other four PSAs. It leads to the reduced coupling effect as well as weak robustness.

Fig. 9 illustrates the RMSE versus the number of snapshots with SNR=10 dB. The proposed GLA-OEL performs the best among all the PSAs, followed by the LA, LdA, HA, HOBA-2 2DNA and 2DCA. To compare the redundancy of adjacent sensors, Fig. 10 presents the RMSE versus mutual coupling effect c_1. As c_1 increases, the estimation

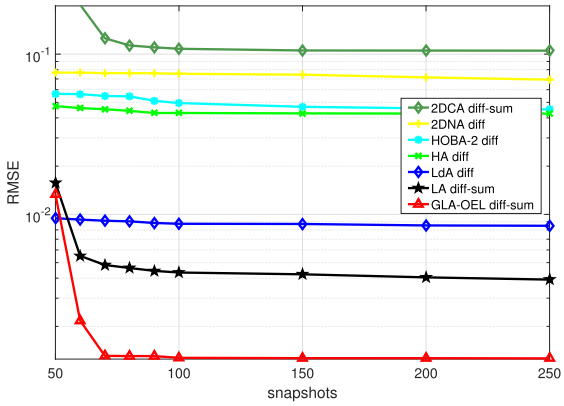

FIGURE 9. RMSE v.s. snapshots with $B = 2$, $c_1 = 0.6$. The SNR is 10 dB.

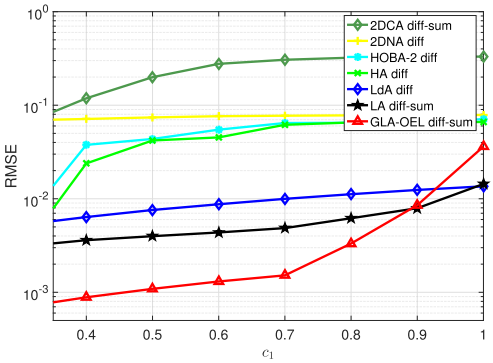

FIGURE 10. RMSE v.s. c_1 with SNR=10 dB and $N_s = 100$.

results get worse for all the PSAs. HOBA-2, HA and 2DCA suffers degration when c_1 is larger than 0.4. While for LA and GLA-OEL, the performance declines severely when $c_1 > 0.8$. It demonstrates that the new structure has the smallest number of sensor pairs located near to each other. At the same time, the DOF is increased dramatically.

VI. CONCLUSION

In this paper, VCAM algorithm is applied onto the traditional L-shaped array to acquire the diff-sum coarray. Due to the special structure of LA, the number of sensor pairs with the separations in each direction except the horizontal and vertical ones can be greatly reduced. As a result, with the same number of sensors used, the increase of DOF can be achieved. To further reduce the redundancy on the x and y axes, an element moving strategy of LA is proposed. By moving any one or more sensors to the centrosymmetric positions, the DSCA will keep intact. Based on this strategy, a generalized L-shaped concept is proposed. Furthermore, the GLA-OEL configuration is presented as a special case of GLA. By moving the even position elements on the positive axes to the mirrored places, the new structure can acquire the lowest weight functions. Combined with the increase of DOF, as a result, more sources can be detected by the GLA-OEL with the mutual coupling considered.

APPENDIX A
PROOF OF PROPERTY 1

1) Denote $\mathbb{D}_{\mathbb{A},\mathbb{B}} = \{\pm(\boldsymbol{p}_i - \boldsymbol{p}_j)|\boldsymbol{p}_i \in \mathbb{A}, \boldsymbol{p}_j \in \mathbb{B}\}$ and $\mathbb{S}_{\mathbb{A},\mathbb{B}} = \{\pm(\boldsymbol{p}_i + \boldsymbol{p}_j)|\boldsymbol{p}_i \in \mathbb{A}, \boldsymbol{p}_j \in \mathbb{B}\}$. Then, according to the definitions of co-arrays in Eq. (8) as well as the expression of LA in Eq. (10), one can obtain that

$$\mathbb{DS}_{LA} = \mathbb{D}_{\mathbb{H},\mathbb{H}} \cup \mathbb{D}_{\mathbb{V},\mathbb{V}} \cup \mathbb{D}_{\mathbb{H},\mathbb{V}} \cup \mathbb{S}_{\mathbb{H},\mathbb{H}} \cup \mathbb{S}_{\mathbb{V},\mathbb{V}} \cup \mathbb{S}_{\mathbb{H},\mathbb{V}}. \tag{21}$$

Substituting the expression of $\mathbb{H}$ and $\mathbb{V}$ into Eq. (21), we have

$$\begin{aligned}
\mathbb{D}_{\mathbb{H},\mathbb{H}} &= \{(n_x, 0)|n_x \in [-N_x, N_x]\};\\
\mathbb{D}_{\mathbb{V},\mathbb{V}} &= \{(0, n_y)|n_y \in [-N_y, N_y]\};\\
\mathbb{D}_{\mathbb{H},\mathbb{V}} &= \{(n_x, n_y)|n_x \in [0, N_x], n_y \in [-N_y, 0]\}\\
&\quad \cup \{(n_x, n_y)|n_x \in [-N_x, 0], n_y \in [0, N_y]\};\\
\mathbb{S}_{\mathbb{H},\mathbb{H}} &= \{(n_x, 0)|n_x \in [-2N_x, 2N_x]\};\\
\mathbb{S}_{\mathbb{V},\mathbb{V}} &= \{(0, n_y)|n_y \in [0, 2N_y] \cup [-2N_y, 0]\};\\
\mathbb{S}_{\mathbb{H},\mathbb{V}} &= \{(n_x, n_y)|n_x \in [0, N_x], n_y \in [0, N_y]\}\\
&\quad \cup \{(n_x, n_y)|n_x \in [-N_x, 0], n_y \in [-N_y, 0]\}.
\end{aligned} \tag{22}$$

It is not difficult to deduce that the cross sum co-array $\mathbb{S}_{\mathbb{H},\mathbb{V}}$ generates the virtual elements in the first and third quadrant. While the cross difference co-array can obtain the second and fourth quadrant elements. The ones at the axes are included in the self sum and self difference results. From Eq. (22) we conclude that a virtual URA at $\mathbb{U}_{LA} = \{(n_x, n_y)|-N_x \le n_x \le N_x, -N_y \le n_y \le N_y\}$ of size $(2N_x+1)\times(2N_y+1)$ is included in the SDCA.

2) Due to the definition of LA in Eq. (10), only one sensor pair contributes to $w(-1, 1)$, i.e., $(0, 1)$, $(1, 0)$. No sensor pair can generate $(1, 1)$. For $w(1, 0)$, the sensors $(i, 0)$, $(i-1, 0)$ with $i = 1, \ldots, N_x$ contribute to it. Therefore, $w(1, 0) = N_x$. Similarly, we have $w(0, 1) = N_y$.

APPENDIX B
PROOF OF LEMMA 1

Denote the original PSA as $\mathbb{P} = \{\boldsymbol{p}_1, \boldsymbol{p}_2, \ldots, \boldsymbol{p}_N\}$ with $\boldsymbol{p}_i = (n_{xi}, n_{yi})$ for $i = 1, 2, \ldots, N$. According to the assumption above Lemma 1, Q sensors at position $\mathbb{S}_1 = \{\boldsymbol{p}_1, \ldots, \boldsymbol{p}_Q\}$ are move to the mirrored places $\widehat{\mathbb{S}}_1 = \{-\boldsymbol{p}_1, \ldots, -\boldsymbol{p}_Q\}$ with the left elements located at $\widehat{\mathbb{S}}_2 = \mathbb{S}_2 = \{\boldsymbol{p}_{Q+1}, \ldots, \boldsymbol{p}_N\}$. Therefore, sensors in the new PSA can be divided into two groups, i.e. $\widehat{\mathbb{P}} = \widehat{\mathbb{S}}_1 \cup \widehat{\mathbb{S}}_2$. While the original PSA can be expressed as $\mathbb{P} = \mathbb{S}_1 \cup \mathbb{S}_2 = (-\widehat{\mathbb{S}}_1) \cup \mathbb{S}_2$. Therefore, the new DSCA can be written as

$$\widehat{\mathbb{DS}} = \mathbb{DS}_{\widehat{\mathbb{S}}_1,\widehat{\mathbb{S}}_1} \cup \mathbb{DS}_{\widehat{\mathbb{S}}_1,\widehat{\mathbb{S}}_2} \cup \mathbb{DS}_{\widehat{\mathbb{S}}_2,\widehat{\mathbb{S}}_2}. \tag{23}$$

Denote $\mathbb{DS}_{\mathbb{A},\mathbb{B}} = \mathbb{D}_{\mathbb{A},\mathbb{B}} \cup \mathbb{S}_{\mathbb{A},\mathbb{B}}$. The analysis of $\widehat{\mathbb{DS}}$ can be divided into three cases. According to the definitions of DSCA, SCA and DCA in Eq. (8), we have

$$\begin{aligned}
\mathbb{DS}_{\widehat{\mathbb{S}}_1,\widehat{\mathbb{S}}_1} &= \mathbb{D}_{\widehat{\mathbb{S}}_1,\widehat{\mathbb{S}}_1} \cup \mathbb{S}_{\widehat{\mathbb{S}}_1,\widehat{\mathbb{S}}_1}\\
&= \{\boldsymbol{p}_i - \boldsymbol{p}_j\} \cup \{\boldsymbol{p}_i + \boldsymbol{p}_j, -\boldsymbol{p}_i - \boldsymbol{p}_j\}
\end{aligned} \tag{24}$$

for $i, j = 1, \ldots, Q$;

$$\begin{aligned}
\mathbb{DS}_{\widehat{\mathbb{S}}_1,\widehat{\mathbb{S}}_2} &= \mathbb{D}_{\widehat{\mathbb{S}}_1,\widehat{\mathbb{S}}_2} \cup \mathbb{S}_{\widehat{\mathbb{S}}_1,\widehat{\mathbb{S}}_2}\\
&= \{\pm(\boldsymbol{p}_i - \boldsymbol{p}_j)\} \cup \{\pm(\boldsymbol{p}_i + \boldsymbol{p}_j)\}
\end{aligned} \tag{25}$$

for $i = 1, \ldots, Q, j = Q+1, \ldots, N$;

$$\begin{aligned}
\mathbb{DS}_{\widehat{\mathbb{S}}_2,\widehat{\mathbb{S}}_2} &= \mathbb{D}_{\widehat{\mathbb{S}}_2,\widehat{\mathbb{S}}_2} \cup \mathbb{S}_{\widehat{\mathbb{S}}_2,\widehat{\mathbb{S}}_2}\\
&= \{\boldsymbol{p}_i - \boldsymbol{p}_j\} \cup \{\boldsymbol{p}_i + \boldsymbol{p}_j, -\boldsymbol{p}_i - \boldsymbol{p}_j\}
\end{aligned} \tag{26}$$

for $i, j = Q+1, \ldots, N$.

On the other hand, the original DSCA has the form of

$$\mathbb{DS} = \mathbb{DS}_{\mathbb{S}_1,\mathbb{S}_1} \cup \mathbb{DS}_{\mathbb{S}_1,\mathbb{S}_2} \cup \mathbb{DS}_{\mathbb{S}_2,\mathbb{S}_2}. \tag{27}$$

Substituting the relationship $\widehat{\mathbb{S}}_1 = -\mathbb{S}_1$ and $\widehat{\mathbb{S}}_2 = \mathbb{S}_2$ into the above equation, one can find that

$$\begin{aligned}
\mathbb{DS}_{\mathbb{S}_1,\mathbb{S}_1} &= \mathbb{D}_{\mathbb{S}_1,\mathbb{S}_1} \cup \mathbb{S}_{\mathbb{S}_1,\mathbb{S}_1}\\
&= \{\boldsymbol{p}_i - \boldsymbol{p}_j\} \cup \{\boldsymbol{p}_i + \boldsymbol{p}_j, -\boldsymbol{p}_i - \boldsymbol{p}_j\}\\
&= \mathbb{D}_{\widehat{\mathbb{S}}_1,\widehat{\mathbb{S}}_1} \cup \mathbb{S}_{\widehat{\mathbb{S}}_1,\widehat{\mathbb{S}}_1} = \mathbb{DS}_{\widehat{\mathbb{S}}_1,\widehat{\mathbb{S}}_1},
\end{aligned} \tag{28}$$

for $i, j = 1, \ldots, Q$;

$$\begin{aligned}
\mathbb{DS}_{\mathbb{S}_1,\mathbb{S}_2} &= \mathbb{D}_{\mathbb{S}_1,\mathbb{S}_2} \cup \mathbb{S}_{\mathbb{S}_1,\mathbb{S}_2}\\
&= \{\pm(\boldsymbol{p}_i - \boldsymbol{p}_j) \cup \{\pm(\boldsymbol{p}_i + \boldsymbol{p}_j)\}\\
&= \mathbb{S}_{\widehat{\mathbb{S}}_1,\widehat{\mathbb{S}}_2} \cup \mathbb{D}_{\widehat{\mathbb{D}}_1,\widehat{\mathbb{D}}_2} = \mathbb{DS}_{\widehat{\mathbb{S}}_1,\widehat{\mathbb{S}}_2}
\end{aligned} \tag{29}$$

for $i = 1, \ldots, Q, j = Q+1, \ldots, N$;

$$\mathbb{DS}_{\mathbb{S}_2,\mathbb{S}_2} = \mathbb{DS}_{\widehat{\mathbb{S}}_2,\widehat{\mathbb{S}}_2}. \tag{30}$$

In conclusion, we have $\widehat{\mathbb{DS}} = \mathbb{DS}$.

REFERENCES

[1] H. V. Trees, *Optimum Array Processing : Part IV Detection, Estimation Modulation Theory*. New York, NY, USA: Wiley, 2002.
[2] H. Krim and M. Viberg, "Two decades of array signal processing research: The parametric approach," *IEEE Signal Process. Mag.*, vol. 13, no. 4, pp. 67–94, 1996.
[3] B. Friedlander and A. J. Weiss, "Direction finding in the presence of mutual coupling," *IEEE Trans. Antennas Propag.*, vol. 39, no. 3, pp. 273–284, Mar. 1991.
[4] Z. Ye, J. Dai, X. Xu, and X. Wu, "DOA estimation for uniform linear array with mutual coupling," *IEEE Trans. Aerosp. Electron. Syst.*, vol. 45, no. 1, pp. 280–288, Jan. 2009.
[5] B. Liao, Z.-G. Zhang, and S.-C. Chan, "DOA estimation and tracking of ULAs with mutual coupling," *IEEE Trans. Aerosp. Electron. Syst.*, vol. 48, no. 1, pp. 891–905, Jan. 2012.
[6] A. Moffet, "Minimum-redundancy linear arrays," *IEEE Trans. Antennas Propag.*, vol. AP-16, no. 2, pp. 172–175, Mar. 1968.
[7] P. Pal and P. P. Vaidyanathan, "Nested arrays: A novel approach to array processing with enhanced degrees of freedom," *IEEE Trans. Signal Process.*, vol. 58, no. 8, pp. 4167–4181, Aug. 2010.
[8] P. P. Vaidyanathan and P. Pal, "Sparse sensing with co-prime samplers and arrays," *IEEE Trans. Signal Process.*, vol. 59, no. 2, pp. 573–586, Feb. 2011.
[9] T.-J. Shan, M. Wax, and T. Kailath, "On spatial smoothing for direction-of-arrival estimation of coherent signals," *IEEE Trans. Acoust., Speech, Signal Process.*, vol. ASSP-33, no. 4, pp. 806–811, Aug. 1985.
[10] J. Liu, Y. Zhang, Y. Lu, S. Ren, and S. Cao, "Augmented nested arrays with enhanced DOF and reduced mutual coupling," *IEEE Trans. Signal Process.*, vol. 65, no. 21, pp. 5549–5563, Nov. 2017.
[11] M. Yang, L. Sun, X. Yuan, and B. Chen, "Improved nested array with hole-free DCA and more degrees of freedom," *Electron. Lett.*, vol. 52, no. 25, pp. 2068–2070, Dec. 2016.

[12] Z. Zheng, W.-Q. Wang, Y. Kong, and Y. D. Zhang, "MISC array: A new sparse array design achieving increased degrees of freedom and reduced mutual coupling effect," *IEEE Trans. Signal Process.*, vol. 67, no. 7, pp. 1728–1741, Apr. 2019.
[13] P. Zhao, G. Hu, Z. Qu, and L. Wang, "Enhanced nested array configuration with hole-free co-array and increasing degrees of freedom for DOA estimation," *IEEE Commun. Lett.*, vol. 23, no. 12, pp. 2224–2228, Dec. 2019.
[14] S. Ren, W. Dong, X. Li, W. Wang, and X. Li, "Extended nested arrays for consecutive virtual aperture enhancement," *IEEE Signal Process. Lett.*, vol. 27, pp. 575–579, 2020.
[15] Y. D. Zhang, M. G. Amin, and B. Himed, "Sparsity-based DOA estimation using co-prime arrays," in *Proc. IEEE Int. Conf. Acoust., Speech Signal Process.*, May 2013, pp. 3967–3971.
[16] C.-L. Liu and P. P. Vaidyanathan, "Super nested arrays: Linear sparse arrays with reduced mutual coupling—Part I: Fundamentals," *IEEE Trans. Signal Process.*, vol. 64, no. 15, pp. 3997–4012, Aug. 2016.
[17] C.-L. Liu and P. P. Vaidyanathan, "Super nested arrays: Linear sparse arrays with reduced mutual coupling—Part II: high-order extensions," *IEEE Trans. Signal Process.*, vol. 64, no. 16, pp. 4203–4217, Aug. 2016.
[18] Q. Shen, W. Liu, W. Cui, S. Wu, and P. Pal, "Simplified and enhanced multiple level nested arrays exploiting high-order difference co-arrays," *IEEE Trans. Signal Process.*, vol. 67, no. 13, pp. 3502–3515, Jul. 2019.
[19] X. Zhang, Y. Wang, and W. Zheng, "Direction of arrival estimation of non-circular signals using modified nested array," in *Proc. IEEE 11th Sensor Array Multichannel Signal Process. Workshop (SAM)*, Jun. 2020, pp. 1–5.
[20] G. Qin, Y. D. Zhang, and M. G. Amin, "DOA estimation exploiting moving dilated nested arrays," *IEEE Signal Process. Lett.*, vol. 26, no. 3, pp. 490–494, Mar. 2019.
[21] G. Qin and M. G. Amin, "Optimum sparse array configuration for DOA estimation on moving platforms," *Digit. Signal Process.*, vol. 2020, Feb. 2020, Art. no. 102685. [Online]. Available: http://www.sciencedirect.com/science/article/pii/S1051200420300300
[22] Z. Zheng, Y. Huang, W.-Q. Wang, and H. C. So, "Spatial smoothing PAST algorithm for DOA tracking using difference coarray," *IEEE Signal Process. Lett.*, vol. 26, no. 11, pp. 1623–1627, Nov. 2019.
[23] Z. Zheng, Y. Huang, W.-Q. Wang, and H. C. So, "Direction-of-Arrival estimation of coherent signals via coprime array interpolation," *IEEE Signal Process. Lett.*, vol. 27, pp. 585–589, 2020.
[24] P. Pal and P. P. Vaidyanathan, "Nested arrays in two dimensions, Part I: Geometrical considerations," *IEEE Trans. Signal Process.*, vol. 60, no. 9, pp. 4694–4705, Sep. 2012.
[25] P. Pal and P. P. Vaidyanathan, "Nested arrays in two dimensions, Part II: Application in two dimensional array processing," *IEEE Trans. Signal Process.*, vol. 60, no. 9, pp. 4706–4718, Sep. 2012.
[26] Q. Wu, F. Sun, P. Lan, G. Ding, and X. Zhang, "Two-dimensional direction-of-arrival estimation for co-prime planar arrays: A partial spectral search approach," *IEEE Sensors J.*, vol. 16, no. 14, pp. 5660–5670, Jul. 2016.
[27] W. Zheng, X. Zhang, and H. Zhai, "Generalized coprime planar array geometry for 2-D DOA estimation," *IEEE Commun. Lett.*, vol. 21, no. 5, pp. 1075–1078, May 2017.
[28] X. Zhang, W. Zheng, and W. Chen, "Two-dimensional doa estimation for generalized coprime planar arrays: A fast-convergence trilinear decomposition approach," *Multidim. Syst. Sign. Process.*, vol. 30, pp. 239–256, Apr. 2019.
[29] C.-L. Liu and P. P. Vaidyanathan, "Two-dimensional sparse arrays with hole-free coarray and reduced mutual coupling," in *Proc. 50th Asilomar Conf. Signals, Syst. Comput.*, Nov. 2016, pp. 1508–1512.
[30] C.-L. Liu and P. P. Vaidyanathan, "Hourglass arrays and other novel 2-D sparse arrays with reduced mutual coupling," *IEEE Trans. Signal Process.*, vol. 65, no. 13, pp. 3369–3383, Jul. 2017.
[31] S. Ren, X. Li, X. Luo, and W. Wang, "Extensions of open box array with reduced mutual coupling," *IEEE Sensors J.*, vol. 18, no. 13, pp. 5475–5484, Jul. 2018.
[32] X. Wang, Z. Chen, S. Ren, and S. Cao, "DOA estimation based on the difference and sum coarray for coprime arrays," *Digit. Signal Process.*, vol. 69, pp. 22–31, Oct. 2017. http://www.sciencedirect.com/science/article/pii/S1051200417301276
[33] J. Shi, G. Hu, X. Zhang, F. Sun, and H. Zhou, "Sparsity-based two-dimensional DOA estimation for coprime array: From sum–difference coarray viewpoint," *IEEE Trans. Signal Process.*, vol. 65, no. 21, pp. 5591–5604, Nov. 2017.
[34] Y. Hua, T. K. Sarkar, and D. D. Weiner, "An L-shaped array for estimating 2-D directions of wave arrival," *IEEE Trans. Antennas Propag.*, vol. 39, no. 2, pp. 143–146, Feb. 1991.
[35] M. D. Zoltowski, M. Haardt, and C. P. Mathews, "Closed-form 2-D angle estimation with rectangular arrays in element space or beamspace via unitary ESPRIT," *IEEE Trans. Signal Process.*, vol. 44, no. 2, pp. 316–328, Feb. 1996.
[36] N. Xi and L. Liping, "A computationally efficient subspace algorithm for 2-D DOA estimation with L-shaped array," *IEEE Signal Process. Lett.*, vol. 21, no. 8, pp. 971–974, Aug. 2014.

XIANGNAN LI received the B.Eng. degree in information engineering from the Beijing Institute of Technology, Beijing, China, in 2016, where he is currently pursuing the Ph.D. degree in electronics science and technology. His research interests include array signal processing and direction of arrival estimation based on virtual arrays.

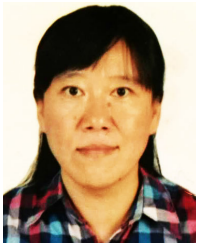

XIAOHUA WANG received the B.Eng. degree in automation and instrument detection technology, in 1993, and the Ph.D. degree in control theory and control engineering from Northeastern University, in 1999. She was a Postdoctoral Researcher at the Chinese Academy of Sciences, in 1999. In 2001, she joined the School of Information and Electronics, Beijing Institute of Technology. Her research interests include nonlinear system theory, array signal processing, and image processing.

WEIJIANG WANG received the B.Eng. and Ph.D. degrees in communication and information system from the Beijing Institute of Technology, Beijing, China, in 1999 and 2004, respectively. In 2004, he joined the faculty of the School of Information and Electronics, Beijing Institute of Technology. His research interests include image processing and array signal processing.

SHIWEI REN received the B.Eng. degree in information engineering from the Beijing Institute of Technology, Beijing, China, in 2008, and the Ph.D. degree in signal and information processing from the University of Chinese Academy of Sciences, Beijing, in 2013. In 2013, she joined the Faculty of the School of Information and Electronics, Beijing Institute of Technology. Her current research interests include direction of arrival estimation, sparse array design, and array signal processing.